RAV12 Accelerates the Desensitization of Akt/PKB Pathway of Insulin-like Growth Factor I Receptor Signaling in COLO205

Jonathan Chi-Hang Li and Ronghao Li

Raven Biotechnologies, Inc., South San Francisco, California

Abstract

RAV12 is a high-affinity immunoglobulin G_1 (IgG_1) chimeric antibody recognizing an N-linked carbohydrate epitope expressed on a number of human carcinomas and adenocarcinomas. RAV12 is efficacious in treating colon, gastric, and pancreatic tumors in xenograft models *in vivo*. Insulin-like growth factor-I receptor (IGF-IR) is a protein widely overexpressed in tumor-derived cell lines that promotes cell survival and prevents apoptosis. We found the RAV12 epitope (RAAG12) decorated the IGF-IR proteins of RAV12-responsive cell lines such as COLO201, COLO205, and SNU-16. Here, we report findings of IGF-IR signaling manipulation by RAV12. We found that RAV12 caused a significantly accelerated IGF-I–mediated IGF-IR phosphorylation and desensitization in COLO205. We also observed significant changes in some of the major downstream signaling components of IGF-IR. Data suggested that RAV12 treatment accelerated the desensitization of Akt/PKB through IRS1, and such activation could be attenuated by Tyrphostin AG538 (IGF-IR inhibitor), LY294002, or Wortmannin (phosphoinositide-3-kinase inhibitor). Furthermore, RAV12-inhibited IGF-I stimulated COLO205 growth, and the inhibition could be significantly augmented by mitogen-activated protein kinase inhibitor. [Cancer Res 2007;67(18):8856–64]

Introduction

Research on cell signaling in cancer biology has provided invaluable information supporting the development of antibody-based therapy. For instance, studies on ErbB oncogenes led to two highly efficacious antibody therapeutics: Herceptin for HER2-overexpressing breast cancer and Erbitux for epidermal growth factor receptor (EGFR)–expressing colorectal and lung cancers (1, 2). Given the existence of EGFR/insulin-like growth factor-IR (IGF-IR) crosstalk (3, 4), the dependence of EGFR on IGF-IR pathway (5, 6) and the role of IGF-I/IGF-IR signaling in regulating cell transformation, tumorigenesis, and apoptosis (7, 8), IGF-IR may be a target for future therapeutic development (9, 10).

IGF-IR is a tetrameric glycoprotein made up of two disulfide-linked heterodimers. Each heterodimer is composed of an extracellular α-subunit, containing the ligand-binding domain, and a transmembrane β-subunit, containing the tyrosine kinase domain and ATP binding cassette (11, 12). Upon ligand binding, IGF-IR undergoes autophosphorylation in the β-subunits and subsequently activates IRS1 by phosphorylation. IRS1 then serves as a hub to relay signals to the mitogen-activated protein kinase (MAPK) pathway via growth factor receptor bound protein 2 and/or to the phosphoinositide-3-kinase (PI3K)-Akt/PKB pathway via the p85 regulatory subunit of PI3K (11–13). The interplay of these signaling cascades allows IGF-IR to exert its role in mediating normal cell growth and cell differentiation (8, 11, 12). Overexpression of IGF-I/IGF-IR is associated with many cancers, including but not limited to lung cancer (14), neuroblastoma (15), cervical cancer (16), breast cancer (17), and colorectal cancer (18). It is now evident that IGF-I/IGF-IR signaling is one of the major survival pathways in cells (8, 11, 12). Up-regulation of IGF-I/IGF-IR signaling renders cells resistant to apoptosis under various conditions such as serum withdrawal (19), UVB irradiation (20, 21), IFNγ/tumor necrosis factor α (TNFα) treatment (22), and cytotoxic agents (23, 24). In fact, down-regulation of IGF-I/IGF-IR signaling can inhibit tumorigenesis, reverse transformed phenotype, and induce apoptosis (10, 24).

Numerous attempts have been made to induce apoptosis or growth inhibition in tumors by modification of the IGF-I/IGF-IR signaling by antagonistic antibodies (24, 25), antisense RNA (15, 24, 26, 27), or dominant negative mutants (14, 24, 26, 27). However, targeting a ubiquitously expressed and physiologically important receptor, such as IGF-IR, may well impair its function(s) in healthy cells and potentially create undesirable side effect(s) (28). An alternative approach to this problem is to target cancer-associated, aberrantly expressed carbohydrates on the receptor rather than the peptide backbone. Recent research in the development of EGFR antibody therapeutic has shown the feasibility of exploiting carbohydrate epitopes on the receptor (29–31).

RAV12 is a high-affinity immunoglobulin G_1 (IgG_1) chimeric antibody recognizing RAAG12, an N-linked carbohydrate epitope containing Galβ1-3GlcNAcβ1-3Gal. Immunohistochemistry showed that RAAG12 is expressed in breast, kidney, lung, ovarian, and prostate tumors. RAAG12 is highly expressed in various gastrointestinal tumors, primary and metastatic colorectal tumors. RAAG12 is also expressed in the cytoplasm of some normal exocrine epithelia and on the apical surface of gastrointestinal and ductal epithelium. RAAG12 is neither expressed in normal connective tissues nor in tissues from the cardiovascular, endocrine, hematolymphatic, neuromuscular, and central nervous systems. Bioassays also showed that RAV12 is cytotoxic *in vitro* and antitumorigenic in various gastrointestinal xenograft models *in vivo*. The details of these studies have been discussed elsewhere (32).

In this report, we use IGF-IR and COLO205 as a model system to explore the manipulation of receptor signaling by RAV12. Results indicated that RAV12 enhances IGF-I–mediated IGF-IR phosphorylation and accelerates receptor desensitization. Analysis of downstream signaling components of IGF-IR reveals a similar accelerated desensitization profile of the Akt/PKB pathway. These observations are supported by a functional cell growth assay.

Note: Supplementary data for this article are available at Cancer Research Online (http://cancerres.aacrjournals.org/).

Requests for reprints: Jonathan Chi-Hang Li, Raven Biotechnologies, Inc., 1 Corporate Drive, South San Francisco, CA 94080. Phone: 650-624-2611; Fax: 650-553-9169; E-mail: jchl@ravenbio.com.

doi:10.1158/0008-5472.CAN-07-0971

Materials and Methods

Reagents. Primary antibodies used in the study were purchased from R&D Systems, Upstate, and Zymed Laboratories. Enzyme-conjugated secondary antibodies were from Jackson ImmunoResearch and Vector Laboratories. Dynabeads Protein-G and Dynabeads goat anti-mouse IgG were from Dynal Biotech. Tyrphostin AG538, PD98059, LY294002, and Wortmannin were from Calbiochem. Cell culture reagents and protein electrophoresis reagents were obtained from Invitrogen. Recombinant human IGF-I was from R&D Systems. Tissue culture plasticwares were from BD Biosciences. Enhanced chemiluminescence (ECL) detection kit was from Amersham Biosciences. One-step nitroblue tetrazolium (NBT)/5-bromo-4-chloro-3-indolyl phosphate (BCIP) solution, bicinchoninic acid (BCA) protein assay kit, and Restore Western blot stripping buffer was from Pierce Biotechnology. SureBlue TMB substrate kit was from Kirkegaard & Perry Laboratories. Radioimmunoprecipitation assay buffer (RIPA), Protease inhibitor cocktail, protein phosphatase inhibitor set, Beadlyte cell signaling buffer kit, and Beadmate antibodies were from Upstate. CellTiter 96 AQueous one solution cell proliferation assay was from Promega. All other chemicals were from Sigma.

Cell lines and cultures. A549, lung carcinoma cell line; CaKi2, renal carcinoma cell line; SNU-16, gastric carcinoma cell line; SU.86.86, pancreas ductal carcinoma cell line; COLO201, COLO205, and HT-29, colorectal adenocarcinoma cell lines were obtained from the American Type Culture Collection (ATCC). Cells were maintained in F12/DMEM supplemented with 10% heat-inactivated fetal bovine serum (FBS, Hyclone) and 50 μg/mL gentamicin. These cultures were incubated in a 37°C incubator with humidified atmosphere of 5% CO_2. Cell cultures used in this study were 2 to 15 passages from thaw of the ATCC vial.

For serum starvation, cells were washed twice with F12/DMEM and cultured in serum-free F12/DMEM at 37°C for 16 to 20 h. The medium was changed, and cells were ready to receive different treatments. Kinase inhibitors such as Tyrphostin AG538, PD98059, LY294002, and Wortmannin were reconstituted in DMSO and kept frozen at −20°C. RAV12, IGF-I, and kinase inhibitor were diluted to appropriate concentration in serum-free F12/DMEM immediately before use.

Generation of KID3 and its chimeric antibody, RAV12. The method for generating KID3 monoclonal antibody (Mab) and its chimeric counterpart, RAV12, have been described elsewhere (32).

Distribution of RAAG12 on membrane proteins. Total cell lysate was prepared from subconfluent cultures of A549, CaKi2, COLO201, COLO205, HT-29, SNU-16, and SU.86.86. Approximately 2×10^6 cells were washed twice with PBS and lysed in 1 mL ice-cold modified RIPA buffer (RIPA with protease inhibitors) at 4°C for 15 min. Lysate was cleared by 15,000 × *g* centrifugation at 4°C for 15 min, and protein content was estimated by BCA assay. Sandwich ELISA was used to detect RAAG12 on membrane proteins of these tumor-derived cell lines. Approximately 5 μg/mL of the following antibodies, including EGFR, FGFR2iiib, IFNγR1, IGF-IR, IR, EphA2, platelet-derived growth factor receptor α (PDGFRα), TfR, transforming growth factor βR2 (TGFβR2), TNFαR1, TNFαR2, and ALCAM were coated onto ELISA plates in carbonate-bicarbonate buffer (pH 9.6) at 4°C overnight. The plates were washed and blocked with 1.5% bovine serum albumin (BSA)/PBS for 1 h. Different dilutions of cell lysates were applied to the plates and incubated for 1 h. The plates were washed and incubated with 2.5 μg/mL biotinylated RAV12 for 1 h. After washing, the plates were further incubated with 1/3,000 dilution of streptavidin–horseradish peroxidase conjugates for 1 h. After washing, color was developed using TMB substrate kit. Optical density of the samples was determined at 450 nm and referenced at 650 nm.

Immunodetection of RAAG12 on IGF-IR. Total cell lysate of A549, CaKi2, COLO201, COLO205, HT-29, SNU-16, and SU.86.86 was prepared as described above. The lysate was immunoprecipitated with 4 μg/mL anti–IGF-IR Mab (R&D Systems, clone 33255) and Dynabeads Protein-G at 4°C overnight. The immunoprecipitate was washed, boiled in sample loading buffer, resolved onto 4% to 20% SDS-PAGE under reducing condition and transferred to 0.45-μm nitrocellulose membrane. Nonspecific binding sites on the membrane were blocked with 5% nonfat dry milk in TBST (TBS with 0.05% Tween 20) for 1 h. The presence of RAAG12 on IGF-IR was detected by ECL with 2 μg/mL biotinylated RAV12 and 1/30,000 dilution of streptavidin–horseradish peroxidase conjugates. After ECL detection, the blot was stripped with Restore Western blot stripping buffer according to the manufacturer's protocol. Total IGF-IR in the samples was detected by probing the blot with 2 μg/mL anti–IGF-IR polyclonal antibody, 1/500 dilution of mouse anti-goat IgG(H + L) alkaline phosphatase conjugates and developed with NBT/BCIP.

IGF-IR phosphorylation. COLO205 were seeded into 35-mm dishes, grown to 70% confluency, and serum-starved as described above. For IGF-IR phosphorylation studies, cells were pretreated with 50 μg/mL RAV12 at 37°C for 0 to 8 h. At the end of each time point, cells were washed twice with serum-free F12/DMEM and post-stimulated with 50 ng/mL IGF-I at 37°C for 8 min. Then cells were washed twice with ice-cold PBS to stop the treatment. Total cell lysate prepared in modified RIPA buffer (RIPA with protease inhibitors and protein phosphatase inhibitors) was immunoprecipitated with 4 μg/mL anti–IGF-IR Mab and Dynabeads goat anti-mouse IgG at 4°C overnight. After washing, the immunoprecipitate was subjected to reducing SDS-PAGE, transferred to nitrocellulose membrane, and immunoblotted with 2 μg/mL anti-phosphotyrosine Mab (Upstate, clone 4G10). Phosphotyrosine content on the IGF-IR β-subunit was detected by ECL. Total IGF-IR in the samples was also detected as described above.

For IGF-IR phosphorylation kinetic studies, serum-starved COLO205 were pretreated with 50 μg/mL RAV12 or serum-free F12/DMEM at 37°C for 4 h. At the end of the incubation, cells were washed and post-stimulated with 50 ng/mL IGF-I at 37°C for 0 to 2 h. Total cell lysate was prepared and analyzed as described above.

The desensitization of IGF-IR phosphorylation was also investigated. Serum-starved COLO205 were pretreated with 50 μg/mL RAV12 or serum-free F12/DMEM for 4 h, washed, and stimulated with or without 50 ng/mL IGF-I (Primary IGF-I challenge) at 37°C for 10 min (for RAV12-pretreated samples) or 15 min (for serum-free F12/DMEM-pretreated samples). Cells were washed twice with serum-free F12/DMEM and allowed to rest at 37°C for 20 min. Then cells were restimulated with or without 100 ng/mL IGF-I at 37°C for 10 min (Secondary IGF-I challenge). Total cell lysate was prepared and analyzed as described above. In these experiments, the band intensity of both phosphorylated and total IGF-IR was quantified using Kodak Molecular Imaging Software (Eastman Kodak).

Inhibition of IGF-IR phosphorylation. A cell-free phosphorylation ELISA was adopted to evaluate the inhibition of IGF-IR phosphorylation (33). Briefly, RAV12 or anti–IGF-IR polyclonal antibody at 5 μg/mL each was coated onto ELISA plates in carbonate-bicarbonate buffer (pH 9.6) at 4°C overnight. Plates were washed and blocked with 1.5% BSA/PBS for 1 h. Total cell lysate from serum-starved A549 and COLO205 was prepared in ice-cold Triton lysis buffer [50 mmol/L Tris-Cl (pH 7.5) containing 150 mmol/L NaCl, 1 mmol/L EDTA, 2% Triton X-100, and protease inhibitors]. Different dilutions of cell lysates were applied to the plates and incubated for 1 h. After washing, the plates were preincubated with 10 μmol/L Tyrphostin AG538 (IGF-IR inhibitor) or DMSO control for 30 min. Cell-free phosphorylation was done in kinase buffer [50 mmol/L Tris-Cl (pH 7.5) containing 20 mmol/L $MgCl_2$, 1 mmol/L DTT, protease inhibitors and protein phosphatase inhibitors] in the presence or absence of 100 μmol/L ATP at 30°C for 30 min. After washing, the plates were incubated with 2.5 μg/mL anti–phospho-IGF-IRβ Mab (Upstate, clone JY202) for 1 h and 1/3,000 dilution of goat anti-mouse IgG (Fc-specific) horseradish peroxidase conjugates for 1 h. After washing, color was developed using TMB substrate kit. Optical density of the sample was determined at 450 nm and referenced at 650 nm.

Analysis of downstream signaling components of IGF-IR. Luminex multiplex assay was used to assess the phospho- and total protein of the following signaling components: IRS1, Akt/PKB, Erk/MAPK1/2, p38SAPK, c-jun-NH_2-kinase (JNK)/stress-activated protein kinase 1 (SAPK1), p70S6K, and HSP27 according to manufacturer's protocol. Briefly, COLO205 were serum starved, pretreated with RAV12 or serum-free F12/DMEM, washed, and post-stimulated with IGF-I as described in IGF-IR phosphorylation kinetic studies. The lysate was multiplexed with either phosphospecific or total Beadmate antibodies in filter plates at 4°C overnight. Plates were

washed and incubated with their respective biotinylated Beadmate antibody pairs for 1 h. After washing, the plates were further incubated with Beadlyte cell signal amplification buffer for 10 min and streptavidin-phycoerythrin for 1 h. Samples were analyzed in the Luminex 100 system.

In some studies, serum-starved COLO205 were pretreated with RAV12 plus specific inhibitor such as 50 μmol/L Tyrphostin AG538, 50 μmol/L PD98059, 50 μmol/L LY294002, or 100 nmol/L wortmannin, washed, and post-stimulated with IGF-I in the presence of the same inhibitor. Signaling components such as IRS1, Akt/PKB, Erk/MAPK1/2, and p70S6K were analyzed as described above.

Effect of MAPK and PI3K inhibitor on RAV12 growth inhibition. An optimal dose of IGF-I for use in these studies was determined as follows. Approximately 2×10^4 COLO205 per well were seeded into 96-well plates in serum-free F12/DMEM. After an overnight serum starvation, cells were cultured with 0 to 1,000 ng/mL IGF-I for 3 days. Cell number in the well was assessed by CellTiter 96 AQueous one solution cell proliferation assay according to manufacturer's protocol. Optical density of the samples was determined at 490 nm and referenced at 650 nm.

To study the effect of MAPK and PI3K inhibitor on RAV12 growth inhibition, COLO205 were seeded and serum starved as described above. Cells were incubated with 50 μg/mL RAV12 or serum-free F12/DMEM in the presence or absence of 10 μmol/L LY294002 or 10 μmol/L PD98059. Cells were further cultured in 100 ng/mL IGF-I for 1 to 3 days. At the end of each time point, cell number in the well was assessed as described above.

Statistical analysis. Results obtained from various experiments were analyzed using Microsoft Excel and Prism (GraphPad Software) softwares. Differences were evaluated by ANOVA with Tukey's post-test, and statistical significance was considered when $P < 0.01$.

Results

Distribution of RAAG12 on membrane proteins and IGF-IR. Since RAV12 recognizes an N-linked carbohydrate epitope (32), we first surveyed its distribution on a subset of membrane proteins from different tumor-derived cell lines. ELISA screening revealed that multiple membrane proteins of COLO205 were highly decorated with RAAG12; this is followed by COLO201, SNU-16, and SU.86.86 (Fig. 1*A*). Some of these RAAG12-bearing membrane proteins were IGF-IR, ALCAM, IFNγR1, TfR, IR, EphA2, and EGFR (Fig. 1*A*). We could not detect RAAG12 on membrane proteins of A549, CaKi2, and HT-29 (data not shown) because these cells showed limited RAAG12 expression on their cell surface (32).

To confirm RAAG12 was indeed associated with IGF-IR, IGF-IR in the cell lysate was immunoprecipitated and detected by RAV12. RAAG12-bearing IGF-IR was found in COLO201, COLO205, and SNU-16, but not on A549, CaKi2, HT-29, nor SU.86.86 (Fig. 1*B*). In COLO201 and COLO205, two RAV12-immunoreactive bands at 130 kDa and 95 kDa were detected and corresponded to the IGF-IRα and IGF-IRβ subunit, respectively (Fig. 1*B* and *C*; ref. 12). While in SNU-16, a differentially glycosylated α-subunit at 120 kDa was observed in place of the 130-kDa band (Fig. 1*B* and *C*; ref. 34). To ensure the absence of RAAG12 on IGF-IR was not due to the absence of IGF-IR in the lysate, the blot in Fig. 1*B* was stripped and probed with anti–IGF-IR polyclonal antibody. As shown in Fig. 1*C*, IGF-IR was found in every cell line. These data seemingly suggest that the decoration of RAAG12 on a subset of membrane proteins,

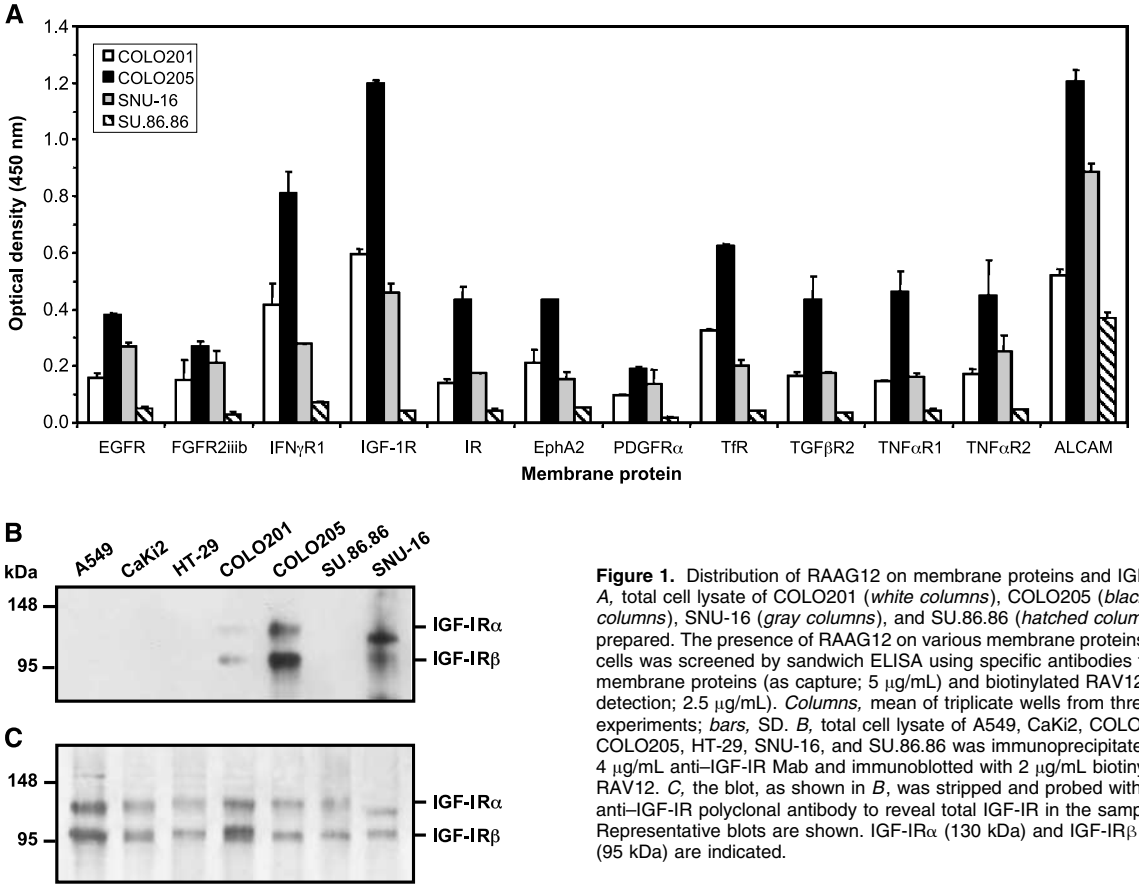

Figure 1. Distribution of RAAG12 on membrane proteins and IGF-IR. *A,* total cell lysate of COLO201 (*white columns*), COLO205 (*black columns*), SNU-16 (*gray columns*), and SU.86.86 (*hatched columns*) was prepared. The presence of RAAG12 on various membrane proteins in these cells was screened by sandwich ELISA using specific antibodies to membrane proteins (as capture; 5 μg/mL) and biotinylated RAV12 (as detection; 2.5 μg/mL). *Columns,* mean of triplicate wells from three experiments; *bars,* SD. *B,* total cell lysate of A549, CaKi2, COLO201, COLO205, HT-29, SNU-16, and SU.86.86 was immunoprecipitated with 4 μg/mL anti–IGF-IR Mab and immunoblotted with 2 μg/mL biotinylated RAV12. *C,* the blot, as shown in *B*, was stripped and probed with 2 μg/mL anti–IGF-IR polyclonal antibody to reveal total IGF-IR in the samples. Representative blots are shown. IGF-IRα (130 kDa) and IGF-IRβ subunits (95 kDa) are indicated.

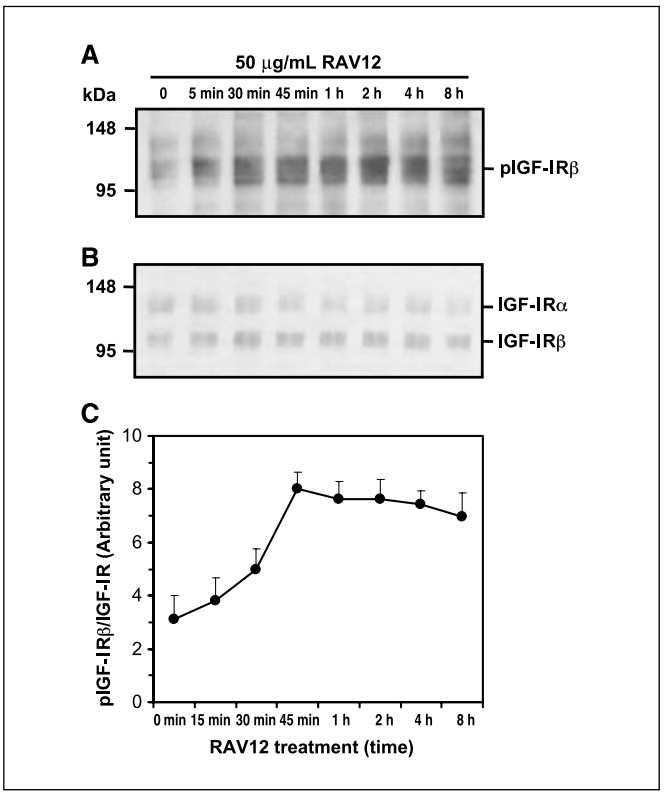

Figure 2. RAV12 enhances IGF-I–mediated IGF-IR phosphorylation. *A,* serum-starved COLO205 were pretreated with 50 μg/mL RAV12 for 0 to 8 h. At the end of each time point, cells were washed and post-stimulated with 50 ng/mL IGF-I for 8 min. Total cell lysate was prepared, immunoprecipitated with 4 μg/mL anti–IGF-IR Mab, and immunoblotted with 2 μg/mL anti-phosphotyrosine Mab. *B,* the blot, as shown in *A*, was stripped and probed with 2 μg/mL anti–IGF-IR polyclonal antibody to reveal total IGF-IR in the samples. Representative blots are shown. Phosphorylated IGF-IR β-subunit (*pIGF-IRβ*), IGF-IRα and IGF-IRβ subunits are indicated. *C,* the phosphorylation level of pIGF-IRβ, as shown in *A*, was normalized to total IGF-IR level, as shown in *B*. Results are expressed as pIGF-IRβ/IGF-IR (mean ± SD) from six experiments.

such as IGF-IR, is a selective process and is unlikely attributed to random events.

Effect of RAV12 on IGF-IR phosphorylation. To understand how RAV12 affects the growth of COLO205, we examined whether RAV12 can manipulate IGF-IR phosphorylation. When COLO205 were pretreated with RAV12 and post-stimulated with IGF-I, an enhancement in IGF-IR phosphorylation of the β-subunit was seen (Fig. 2*A* and *C*). Multiple species of phosphorylated β-subunit was observed at about 95 kDa (Fig. 2*A*). However, RAV12 pretreatment alone was unable to alter basal IGF-IR phosphorylation when IGF-I post-stimulation was omitted (Fig. 4*A, i* at 0 min). We also found that RAV12-enhanced, IGF-I–mediated IGF-IR phosphorylation was not associated with changes in the total amount of IGF-IR (Fig. 2*B*). The lack of changes in total IGF-IR proteins after receptor phosphorylation has been reported previously (35–38).

Inhibition of IGF-IR phosphorylation. To determine whether the RAV12-enhanced, IGF-I–mediated IGF-IR phosphorylation is a specific event, Tyrphostin AG538 (IGF-IR inhibitor) was included in the above phosphorylation studies. Due to high intracellular substrate level, we could not detect any significant decrease in IGF-IR phosphorylation by immunoprecipitation and immunoblot procedures. Hence, we employed a cell-free phosphorylation ELISA to address this question (33). Results indicated that IGF-IR phosphorylation was significantly inhibited by 10 μmol/L Tyrphostin AG538 with inhibition level comparable to "no ATP" phosphorylation. No IGF-IR phosphorylation was observed in A549 lysate captured with RAV12 (Fig. 3). The failure of RAV12-captured A549 lysate to yield IGF-IR phosphorylation is consistent with the fact that A549 contains no RAAG12-bearing IGF-IR (Fig. 1*B*). In contrast, a comparable *in vitro* phosphorylation profile was noted in COLO205 regardless of capture antibody used (Fig. 3).

Effect of RAV12 on kinetics of IGF-IR phosphorylation. Next, we compared IGF-IR phosphorylation kinetics in the presence of RAV12. RAV12-pretreated, IGF-I–stimulated COLO205 exhibited significant, transient increase in IGF-IR phosphorylation (Fig. 4*A, i* and *v*). The increase occurred at 5 min post IGF-I stimulation and was in decline by 15 min. Thereafter, IGF-IR phosphorylation remained constantly low over the course of the experiment (Fig. 4*A, i* and *v*). A similar increase in IGF-IR phosphorylation was also detected in COLO205 that received only IGF-I stimulation (Fig. 4*A, iii* and *v*). However, contrary to the time course seen with RAV12 pretreatment, IGF-IR phosphorylation peaked at about 15–20 min following IGF-I stimulation, a 5–10 min delay versus RAV12-pretreated samples. Then IGF-IR phosphorylation declined at a much more gradual rate when compared with RAV12 pretreatment (Fig. 4*A, iii* and *v*).

To correlate whether this RAV12-accelerated, IGF-IR dephosphorylation is due to receptor desensitization, we deliberately restimulated COLO205 after their exposure to primary IGF-IR stimulation. Results indicated that a robust IGF-IR phosphorylation was produced in the absence of RAV12 (Fig. 4*B*). As predicted, IGF-IR became refractory to IGF-I restimulation when COLO205 were previously exposed to both RAV12 and IGF-I (Fig. 4*B*). The phosphorylation levels obtained in these studies were readily comparable to previous observations (Figs. 2; 4*A, v*). Similarly, basal

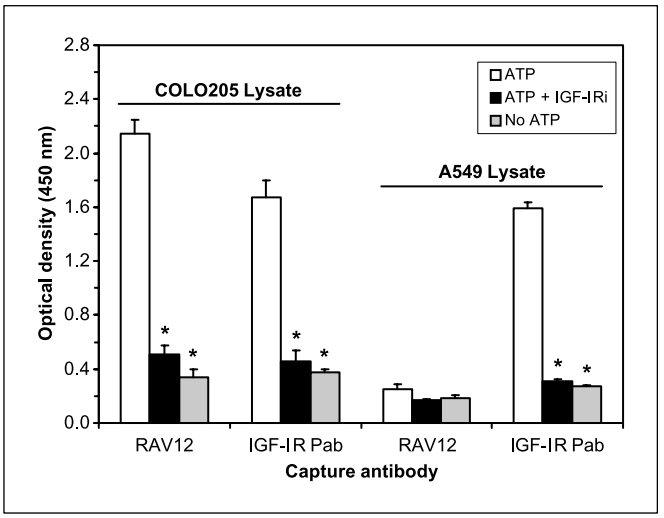

Figure 3. Inhibition of IGF-IR phosphorylation. Total cell lysate from serum-starved A549 and COLO205 was prepared. The lysate was captured by RAV12 (5 μg/mL) or anti-IGF-IR polyclonal antibody (5 μg/mL). Cell-free phosphorylation was done with or without 10 μmol/L Tyrphostin AG538 (*IGF-IRi*) and in the presence (*ATP*) or absence of 100 μmol/L ATP (*No ATP*). Phosphorylated IGF-IR was detected by 2.5 μg/mL anti–Phospho-IGF-IRβ Mab. *Columns,* mean of triplicate wells from three experiments; *bars,* SD. *, $P < 0.01$, statistical significance when compared with phosphorylation done in the presence of ATP alone.

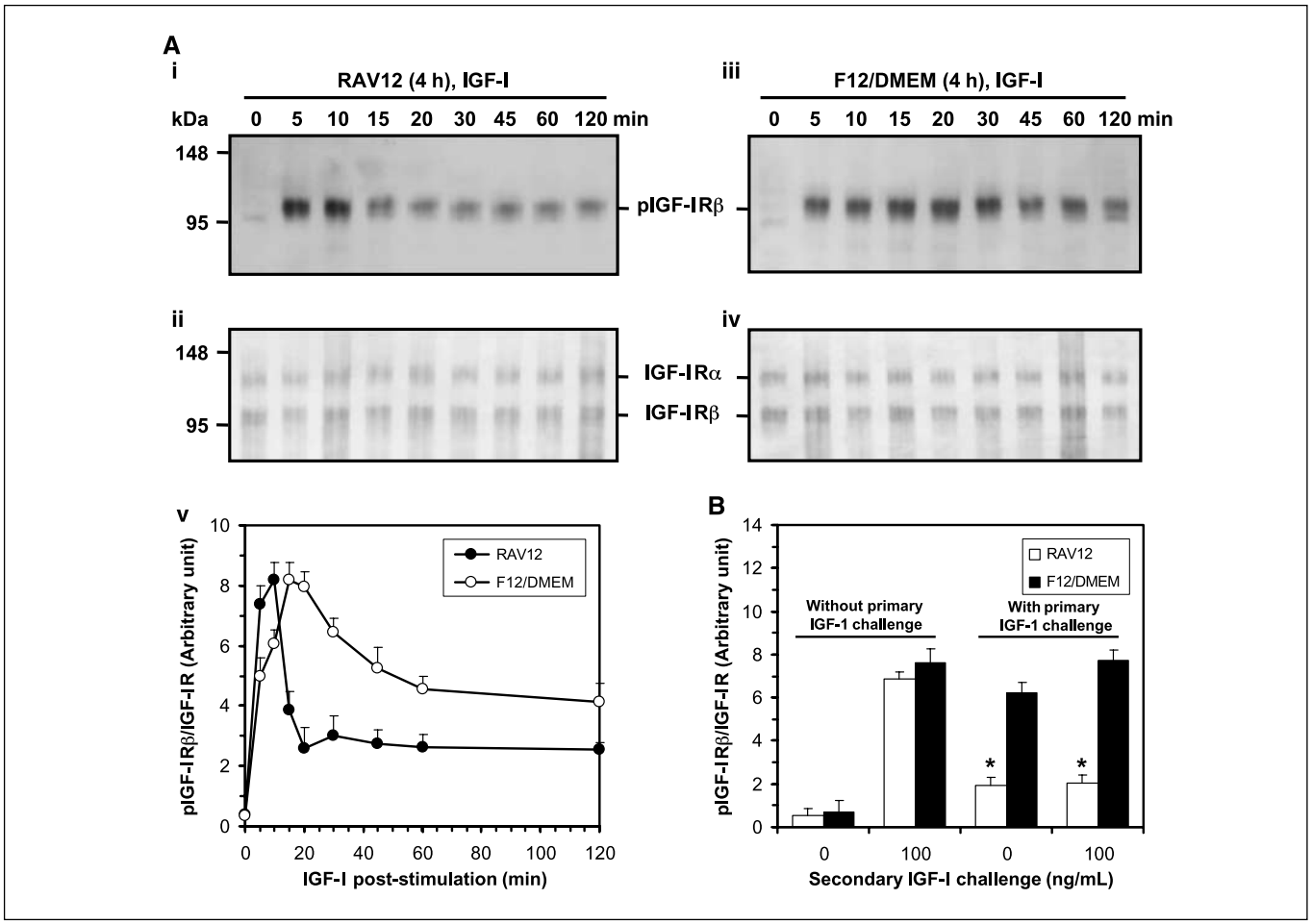

Figure 4. Effect of RAV12 on IGF-IR phosphorylation kinetics. *A,* serum-starved COLO205 were pretreated with 50 μg/mL RAV12 (*i*) or F12/DMEM (*iii*) for 4 h. At the end of incubation, cells were washed and post-stimulated with 50 ng/mL IGF-I for 0 to 2 h. Total cell lysate was prepared and analyzed as described in Materials and Methods. *i* and *iii,* blots immunoprecipitated with 4 μg/mL anti–IGF-IR Mab and probed with 2 μg/mL anti-phosphotyrosine Mab. *ii* and *iv,* the blots, as shown in (*i* and *iii*), were stripped and probed with 2 μg/mL anti–IGF-IR polyclonal antibody to reveal total IGF-IR in the samples. Representative blots are shown. Phosphorylated IGF-IR β-subunit (*pIGF-IRβ*), IGF-IRα, and IGF-IRβ subunits are indicated. *v,* the phosphorylation level of pIGF-IRβ, as shown in *i* and *iii*, was normalized to total IGF-IR level, as shown in *ii* and *iv*, respectively. Results are expressed as pIGF-IRβ/IGF-IR (mean ± SD) from six experiments. *B,* desensitization of IGF-IR phosphorylation by RAV12 was also investigated as follows. Serum-starved COLO205 were pretreated with 50 μg/mL RAV12 or F12/DMEM for 4 h and stimulated with or without 50 ng/mL IGF-I for 10 to 15 min (Primary IGF-I challenge). After washing and 20 min rest in F12/DMEM, cells were restimulated with or without 100 ng/mL IGF-I for 10 min (Secondary IGF-I challenge). Total cell lysate was prepared and analyzed as described in *i–v*. Results are expressed as pIGF-IRβ/IGF-IR (mean ± SD) from three experiments. *, $P < 0.01$, statistical significance when compared with COLO205 received F12/DMEM treatment.

IGF-IR phosphorylation was minimal when IGF-I stimulation was omitted (Fig. 4*A, v* at 0 min; Fig. 4*B* without primary or secondary IGF-I challenge), and no significant changes in total IGF-IR were detected following receptor phosphorylation (Fig. 4*A, ii* and *iv*). Therefore, RAV12 accelerates IGF-IR phosphorylation and causes receptor desensitization.

Analysis of downstream signaling components of IGF-IR. To further explore the effect of RAV12 on IGF-IR intracellular signaling, a series of IGF-IR downstream signaling components was evaluated. The total protein of each signaling component remained constant throughout the experiments (data not shown). We started the analysis with IRS1, Erk/MAPK1/2, Akt/PKB, and p70S6K. IRS1 phosphorylation essentially mirrored the kinetics of IGF-IR phosphorylation (Fig. 4*A, v*). RAV12 pretreatment induced a sharp, transient increase in IRS1 phosphorylation at 10 min to be followed by a sharp decrease and return to the basal level (Fig. 5*A*). Without RAV12 pretreatment, IGF-I stimulation produced a more gradual increase in the IRS1 phosphorylation and followed by a gradual decrease back to the basal level (Fig. 5*A*). Similar trends in Akt/PKB phosphorylation were noted, in which RAV12 quickly accelerated Akt/PKB phosphorylation and desensitization when compared with IGF-I stimulation alone (Fig. 5*B*). Unlike IRS1 phosphorylation, Akt/PKB phosphorylation was never restored to its original level at 2 h (Fig. 5*B*). Apparently, RAV12 could not affect the phosphorylation profile of either Erk/MAPK1/2 or p70S6K (Supplementary Fig. S1*A* and *B*). Nevertheless, unique observations were noted for these components: the basal Erk/MAPK1/2 phosphorylation was unexpectedly high when compared with other signaling components studied (Supplementary Fig. S1*A*), and p70S6K became constitutively active after its initial phosphorylation (Supplementary Fig. S1*B*). We hypothesize these results from the fact that both components are targets of a multitude of kinases activated following IGF-IR phosphorylation (12, 13). For instance, IGF-I trans-activated EGFR (5, 6) or Src homology and collagen (5) can phosphorylate MAPK; atypical PKC (39) or mTOR (40) can phosphorylate p70S6K.

We also studied two stress-activated MAPK pathways frequently associated with IGF-IR signaling, namely, JNK/SPAK1 and p38SAPK (13). JNK/SAPK1, a component that regulates IRS1 phosphorylation (41), revealed no significant changes in its phosphorylation under either condition (data not shown). p38SAPK, a component modified by Akt/PKB (42), revealed a similar accelerated desensitization profile after RAV12 pretreatment (Fig. 5*C*). We also observed a similar trend for HSP27 (Fig. 5*D*), a component distantly downstream to p38SAPK and Akt/PKB (42).

To confirm the effect of RAV12 on IGF-IR intracellular signaling, inhibitors to IGF-IR, MAPK, or PI3K were included in the RAV12 pretreatment. By inhibiting IGF-IR phosphorylation with Tyrphostin AG538 (IGF-IR inhibitor), all the downstream signaling components of IGF-IR examined were significantly inhibited (Supplementary Table S1). On the other hand, PD98059 (MAPK inhibitor), LY294002, or wortmannin (PI3K inhibitor) inhibited only its intended target(s) (Supplementary Table S1). Interestingly, the degree of inhibition by IGF-IR inhibitor was very different from MAPK inhibitor or PI3K inhibitor. Tyrphostin AG538 caused 50% inhibition versus more than 85% inhibition caused by PD98059, LY294002, or wortmannin. Through IGF-IR, RAV12 exerts its effect on a number of intracellular signaling components including, but not limited to, the accelerated desensitization of Akt/PKB pathway.

Effect of MAPK and PI3K inhibitor on RAV12 growth inhibition. We previously showed that RAV12 treatment acts on Akt/PKB pathway of IGF-IR signaling. Therefore, we investigated how this signaling event affects COLO205 growth under IGF-I stimulation. An optimal dose of IGF-I at 100 ng/mL was selected based on the growth characteristic of COLO205 (Fig. 6*A*). Under such condition, RAV12 alone caused a significant growth inhibition on COLO205 (Fig. 6*B*). The combination of RAV12 with MAPK inhibitor generated an additive effect on RAV12 growth inhibition (Fig. 6*B*). We believe this combination produces a dual inhibition of PI3K and MAPK pathways, the two major pathways for cell survival and cell proliferation of IGF-IR signaling. Despite RAV12 and PI3K inhibitor working through the same pathway, their combination generated only a small increase in RAV12 growth inhibition (Fig. 6*B*). One explanation for this may partly be due to the incomplete inhibition of Akt/PKB phosphorylation by

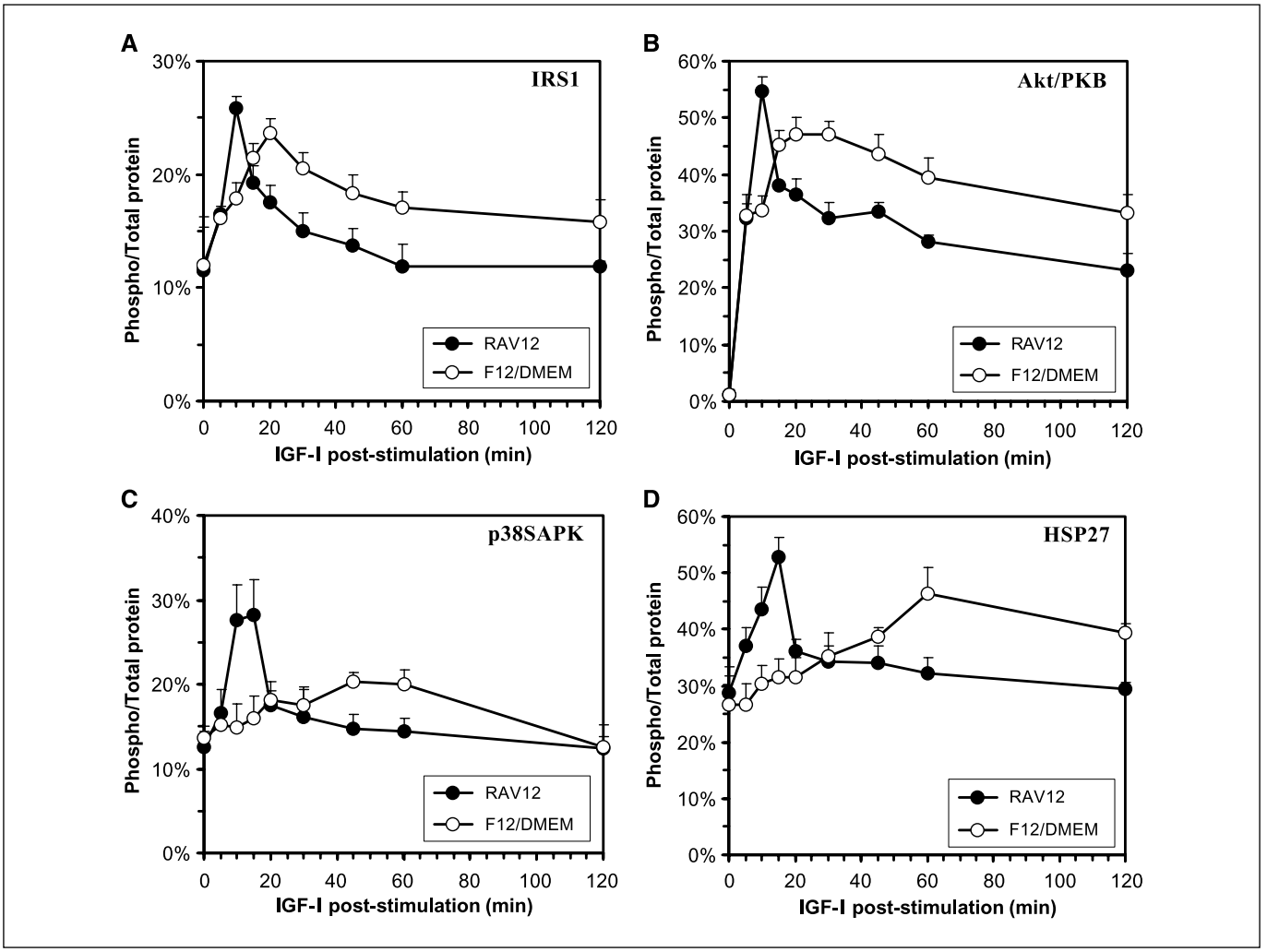

Figure 5. Analysis of downstream signaling components of IGF-IR. Serum-starved COLO205 were pretreated with 50 μg/mL RAV12 (●) or F12/DMEM (○) for 4 h and post-stimulated with 50 ng/mL IGF-I for 0 to 2 h as described in Materials and Methods. Total cell lysate was prepared and four downstream signaling components of IGF-IR such as IRS1 (*A*), Akt/PKB (*B*), p38SAPK (*C*), and HSP27 (*D*) were analyzed by Luminex multiplex assay. Results are expressed as % phospho-protein/total protein (%*P*/*T*, mean ± SD) of duplicate wells from six experiments.

PI3K inhibitor (Supplementary Table S1). In essence, RAV12 inhibits COLO205 growth, and the inhibition can be augmented by MAPK inhibitor.

Discussion

Carbohydrate epitopes, such as those found in mucin-like molecules, glycolipids, or glycoproteins, have been used as markers for cancer diagnosis and prognosis (43, 44). Targeting these carbohydrate epitopes found on the cell surface creates a new class of antibody therapeutics that can selectively recognize tumor-associated antigens and offer broad specificity to various protein targets containing such antigens. However, the therapeutic value of these naked anti-carbohydrate antibodies would be increased with a better understanding of signal transduction events occurring in the target cells. To date, their uses have largely been restricted as toxin- or radio-conjugates (C242-DM4, ImmunoGen, Inc.; anti-Lewis Y, Seattle Genetics, Inc.) due to the minimal, or lack of, activity of these Mabs as naked antibodies. The findings in this report that RAV12, an anti-carbohydrate Mab, can regulate tumor growth, in part, through the manipulation of growth factor receptor(s) suggests a mechanism that might contribute to the development of naked anti-carbohydrate Mabs for cancer therapies.

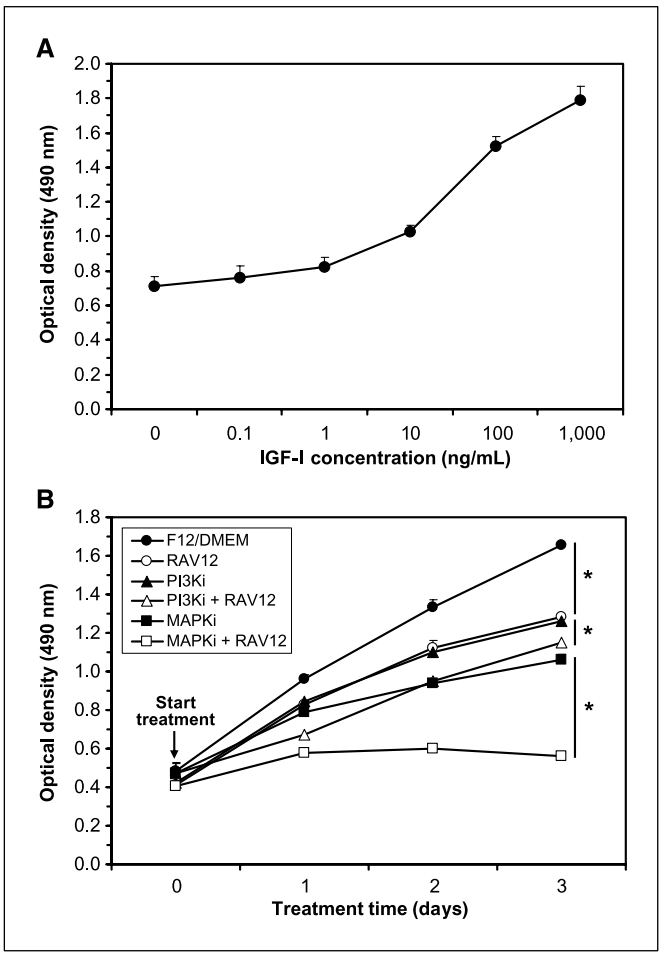

Figure 6. Effect of MAPK and PI3K inhibitor on RAV12 growth inhibition. *A,* COLO205 at 2×10^4 cells per well were serum-starved overnight. Cells were treated with 0 to 1000 ng/mL IGF-I for 3 d. Cell number was assessed as described in Materials and Methods. *B,* serum-starved COLO205 received the following treatments: F12/DMEM (●), 50 μg/mL RAV12 (○), 10 μmol/L LY294002 (*PI3Ki*, ▲), 10 μmol/L LY294002 + 50 μg/mL RAV12 (*PI3Ki + RAV12*, △), 10 μmol/L PD98059 (*MAPKi*, ■), or 10 μmol/L PD98059 + 50 μg/mL RAV12 (*MAPKi + RAV12*, □). Cells continued to grow in the presence of 100 ng/mL IGF-I for 1 to 3 d. Cell number was assessed as described in Materials and Methods. *Points,* mean of triplicate wells from three experiments; *bars,* SD. *, $P < 0.01$, statistical significance when compared with COLO205 received no RAV12 treatment within the same group.

RAV12 recognizes an N-linked carbohydrate epitope expressed on various adenocarcinomas (32). Unlike other known tumor-specific carbohydrate antigens, RAAG12 is shown to be located on a number of well-characterized drug targets such as IGF-IR, IFNγR1, TfR, IR, EphA2, and EGFR in a subset of tumor-derived cell lines (Fig. 1). It is conceivable that RAV12 may modulate the function(s) of one or more such receptors through its binding to the carbohydrate epitope on the receptors, and this may contribute to an eventual inhibition of tumor growth and/or tumor death. Among those RAAG12-bearing receptors, we show that at least one, IGF-IR, is affected by RAV12 (Figs. 2 and 4).

Although RAV12 by itself cannot activate IGF-IR, its binding to COLO205 facilitates the ligand-dependent activation and desensitization of IGF-IR phosphorylation (Figs. 2 and 4). This accelerated desensitization profile of IGF-IR phosphorylation is also reflected in several downstream signaling components such as IRS1, Akt/PKB, and p38SAPK (Fig. 5*A–C*). Akt/PKB is an important interlink on the signaling pathway by integrating extracellular signals from various receptors, such as IGF-IR, to many intracellular signaling molecules including GSK-3, mTOR, p70S6K, BAD, NFκB, and Forkhead (13). Their subsequent phosphorylations allow Akt/PKB to regulate cell survival, proliferation, differentiation, and metabolism (45–47). Therefore, Akt/PKB dysregulation, or persistent activation, is one of the major underlying causes of tumorigenesis, tumor metastasis, and resistance to cancer therapies (45–47). The ability of RAV12 to accelerate the desensitization of IGF-IR and its downstream components, such as Akt/PKB, suggests RAV12 growth inhibition may also work in an Akt/PKB-dependent pathway.

Indeed, results from *in vitro* assay support such a hypothesis. When COLO205 were cultured in the presence of IGF-I, RAV12 significantly inhibits its cell growth. The inhibition can be significantly enhanced by manipulating the IGF-IR signaling with MAPK inhibitor (Fig. 6*B*). It is known that IGF-I/IGF-IR signaling is one of the most responsive pathways in cells of the gastrointestinal tract (48), and most importantly, our studies illustrated that a significant population of IGF-IR is decorated with RAAG12 in some of the RAV12-responsive cell lines (Fig. 1). In essence, the desensitization of IGF-IR signaling should be sufficient to account for a portion of the inhibition of tumor growth.

It was reported that anti-carbohydrate antibodies, such as anti-blood group A carbohydrate Mab (29, 30) or anti-Lewis Y Mab (31), inhibited receptor function of epitope-bearing EGFR. However, it remains uncertain how the binding of RAV12 to a carbohydrate epitope on IGF-IR can induce such changes as described above (Figs. 2 and Figs. 4–6). Results from confocal microscopy studies may offer a possible explanation by showing that RAV12 can aggregate or cross-link RAAG12-bearing membrane protein(s) over time.[1] Because aggregation or cross-linking of membrane proteins is known to activate or sensitize receptors to ligand stimulation (49, 50), we believe that RAV12 may also act on receptor(s) in a similar manner.

[1] Unpublished observations.

However, modulation of IGF-IR signaling may not be the sole mechanism for RAV12 growth inhibition. RAV12 causes a stronger growth inhibition on COLO205 in serum-containing conditions (32) than in IGF-I supplemented serum-free medium. We speculate that the presence of multiple cytokines or growth factors in serum may allow RAV12 to modulate ligand-dependent signaling of other RAAG12-bearing receptor(s) besides IGF-IR. We also believe that RAV12 may exert its activity through a combination of RAAG12-bearing receptor(s) varying across different tumor-derived cell lines.[1] Despite the fact that RAAG12 is present on various receptors on colorectal cancer cell lines (Fig. 1*A*), it is very unlikely that RAV12 will affect normal cellular functions because RAAG12 is undetectable on the same set of receptors such as IGF-IR, ALCAM, IFNγR1, TfR, IR, EphA2, and EGFR in normal adult colon cell lysates.[1] We suspect that the decoration of RAAG12 on receptors may result from the dysregulation of glycosylation pathway in tumor-derived cell lines. Experiments are in progress to further explore this area. In summary, our results clearly indicate that RAV12 affects the Akt/PKB pathway of IGF-IR signaling in COLO205. The fact that RAV12 can target and/or modulate other RAAG12-bearing receptor(s) might be advantageous when compared with other antibody therapeutics currently used in cancer therapies that only target a single, specific receptor.

Acknowledgments

Received 3/14/2007; revised 5/23/2007; accepted 6/20/2007.

The costs of publication of this article were defrayed in part by the payment of page charges. This article must therefore be hereby marked *advertisement* in accordance with 18 U.S.C. Section 1734 solely to indicate this fact.

We thank Tony Liang, Deryk Loo, Jennie Mather, George Schreiner, and Gordon Vehar for their helpful discussions and suggestions. We also thank the Raven Hybridoma, Production, Purification and Cell Biology groups for their excellent technical supports.

References

1. Roskoski R, Jr. The ErbB/HER receptor protein-tyrosine kinases and cancer. Biochem Biophys Res Commun 2004;319:1–11.
2. Ross JS, Schenkein DP, Pietrusko R, et al. Targeted therapies for cancer 2004. Am J Clin Pathol 2004;122:598–609.
3. Coppola D, Ferber A, Miura M, et al. A functional insulin-like growth factor I receptor is required for the mitogenic and transforming activities of the epidermal growth factor receptor. Mol Cell Biol 1994;14:4588–95.
4. Adams TE, McKern NM, Ward CW. Signalling by the type 1 insulin-like growth factor receptor: interplay with the epidermal growth factor receptor. Growth Factors 2004;22:89–95.
5. Roudabush FL, Pierce KL, Maudsley S, et al. Transactivation of the EGF receptor mediates IGF-I–stimulated shc phosphorylation and ERK1/2 activation in COS-7 cells. J Biol Chem 2000;275:22583–9.
6. Mulligan C, Rochford J, Denyer G, et al. Microarray analysis of insulin and insulin-like growth factor-1 (IGF-I) receptor signaling reveals the selective up-regulation of the mitogen heparin-binding EGF-like growth factor by IGF-I. J Biol Chem 2002;277:42480–7.
7. Khandwala HM, McCutcheon IE, Flyvbjerg A, et al. The effects of insulin-like growth factors on tumorigenesis and neoplastic growth. Endocr Rev 2000;21:215–44.
8. Romano G. The complex biology of the receptor for the insulin-like growth factor-1. Drug News Perspect 2003;16:525–31.
9. Brodt P, Samani A, Navab R. Inhibition of the type I insulin-like growth factor receptor expression and signaling: novel strategies for antimetastatic therapy. Biochem Pharmacol 2000;60:1101–7.
10. Bahr C, Groner B. The insulin like growth factor-1 receptor (IGF-IR) as a drug target: novel approaches to cancer therapy. Growth Horm IGF Res 2004;14:287–95.
11. White MF, Kahn CR. The insulin signaling system. J Biol Chem 1994;269:1–4.
12. De Meyts P, Wallach B, Christoffersen CT, et al. The insulin-like growth factor-I receptor. Structure, ligand-binding mechanism and signal transduction. Horm Res 1994;42:152–69.
13. White MF. Insulin Signaling Pathway. Sci STKE (connections map) http://stke.sciencemag.org/ 2005.
14. Lee CT, Park KH, Adachi Y, et al. Recombinant adenoviruses expressing dominant negative insulin-like growth factor-I receptor demonstrate antitumor effects on lung cancer. Cancer Gene Ther 2003;10:57–63.
15. Liu X, Turbyville T, Fritz A, et al. Inhibition of insulin-like growth factor I receptor expression in neuroblastoma cells induces the regression of established tumors in mice. Cancer Res 1998;58:5432–8.
16. Steller MA, Delgado CH, Bartels CJ, et al. Overexpression of the insulin-like growth factor-1 receptor and autocrine stimulation in human cervical cancer cells. Cancer Res 1996;56:1761–5.
17. Kucab JE, Dunn SE. Role of IGF-IR in mediating breast cancer invasion and metastasis. Breast Dis 2003;17:41–7.
18. Wu Y, Yakar S, Zhao L, et al. Circulating insulin-like growth factor-I levels regulate colon cancer growth and metastasis. Cancer Res 2002;62:1030–5.
19. Gil-Ad I, Shtaif B, Luria D, et al. Insulin-like-growth-factor-I (IGF-I) antagonizes apoptosis induced by serum deficiency and doxorubicin in neuronal cell culture. Growth Horm IGF Res 1999;9:458–64.
20. Kulik G, Klippel A, Weber MJ. Antiapoptotic signalling by the insulin-like growth factor I receptor, phosphatidylinositol 3-kinase, and Akt. Mol Cell Biol 1997;17:1595–606.
21. Decraene D, Agostinis P, Bouillon R, et al. Insulin-like growth factor-1–mediated AKT activation postpones the onset of ultraviolet B-induced apoptosis, providing more time for cyclobutane thymine dimer removal in primary human keratinocytes. J Biol Chem 2002;277:32587–95.
22. Remacle-Bonnet MM, Garrouste FL, Heller S, et al. Insulin-like growth factor-I protects colon cancer cells from death factor-induced apoptosis by potentiating tumor necrosis factor α-induced mitogen-activated protein kinase and nuclear factor κB signaling pathways. Cancer Res 2000;60:2007–17.
23. Dunn SE, Hardman RA, Kari FW, et al. Insulin-like growth factor 1 (IGF-I) alters drug sensitivity of HBL100 human breast cancer cells by inhibition of apoptosis induced by diverse anticancer drugs. Cancer Res 1997;57:2687–93.
24. Bahr C, Groner B. The IGF-I receptor and its contributions to metastatic tumor growth-novel approaches to the inhibition of IGF-IR function. Growth Factors 2005;23:1–14.
25. Cohen BD, Baker DA, Soderstrom C, et al. Combination therapy enhances the inhibition of tumor growth with the fully human anti-type 1 insulin-like growth factor receptor monoclonal antibody CP-751,871. Clin Cancer Res 2005;11:2063–73.
26. Resnicoff M, Coppola D, Sell C, et al. Growth inhibition of human melanoma cells in nude mice by antisense strategies to the type 1 insulin-like growth factor receptor. Cancer Res 1994;54:4848–50.
27. Adachi Y, Lee CT, Carbone DP. Genetic blockade of the insulin-like growth factor 1 receptor for human malignancy. Novartis Found Symp 2004;262:177–89.
28. Schneider JW, Chang AY, Rocco TP. Cardiotoxicity in signal transduction therapeutics: erbB2 antibodies and the heart. Semin Oncol 2001;28:18–26.
29. Gregorou M, Rees AR. Properties of a monoclonal antibody to epidermal growth factor receptor with implications for the mechanism of action of EGF. EMBO J 1984;3:929–37.
30. Gooi HC, Picard JK, Hounsell EF, et al. Monoclonal antibody (EGR/G49) reactive with the epidermal growth factor receptor of A431 cells recognizes the blood group ALeb and ALey structures. Mol Immunol 1985;22:689–93.
31. Klinger M, Farhan H, Just H, et al. Antibodies directed against Lewis-Y antigen inhibit signaling of Lewis-Y modified ErbB receptors. Cancer Res 2004;64:1087–93.
32. Loo D, Pryer N, Young P, et al. The glycotope-specific RAV12 monoclonal antibody induces oncosis *in vitro* and has antitumor activity against gastrointestinal adenocarcinoma tumor xenografts *in vivo*. Mol Cancer Ther 2007;6:856–65.
33. Blum G, Gazit A, Levitzki A. Substrate competitive inhibitors of IGF-I receptor kinase. Biochemistry 2000;39:15705–12.
34. Rosenzweig SA, Zetterstrom C, Benjamin A. Identification of retinal insulin receptors using site-specific antibodies to a carboxyl-terminal peptide of the human insulin receptor α-subunit. Up-regulation of neuronal insulin receptors in diabetes. J Biol Chem 1990;265:18030–4.
35. Yamasaki H, Prager D, Melmed S. Structure-function of the human insulin-like growth factor-I receptor: a discordance of somatotroph internalization and signaling. Mol Endocrinol 1993;7:681–5.
36. Prager D, Li HL, Yamasaki H, et al. Human insulin-like growth factor I receptor internalization. Role of the juxtamembrane domain. J Biol Chem 1994;269:11934–7.
37. Stannard B, Blakesley V, Kato H, et al. Single tyrosine substitution in the insulin-like growth factor I receptor inhibits ligand-induced receptor autophosphorylation and internalization, but not mitogenesis. Endocrinology 1995;136:4918–24.
38. Miura M, Baserga R. The tyrosine residue at 1250 of the insulin-like growth factor I receptor is required for ligand-mediated internalization. Biochem Biophys Res Commun 1997;239:182–5.
39. Romanelli A, Martin KA, Toker A, et al. p70 S6 kinase is regulated by protein kinase Cζ and participates in a phosphoinositide 3-kinase–regulated signalling complex. Mol Cell Biol 1999;19:2921–8.
40. Song YH, Godard M, Li Y, et al. Insulin-like growth factor I–mediated skeletal muscle hypertrophy is characterized by increased mTOR-p70S6K signaling without increased Akt phosphorylation. J Investig Med 2005;53:135–42.
41. Mamay CL, Mingo-Sion AM, Wolf DM, et al. An inhibitory function for JNK in the regulation of IGF-I signaling in breast cancer. Oncogene 2003;22:602–14.

42. Rane MJ, Coxon PY, Powell DW, et al. p38 Kinase-dependent MAPKAPK-2 activation functions as 3-phosphoinositide-dependent kinase-2 for Akt in human neutrophils. J Biol Chem 2001;276:3517–23.
43. Byrd JC, Bresalier RS. Mucins and mucin binding proteins in colorectal cancer. Cancer Metastasis Rev 2004;23:77–99.
44. Dabelsteen E. Cell surface carbohydrates as prognostic markers in human carcinomas. J Pathol 1996; 179:358–69.
45. West KA, Castillo SS, Dennis PA. Activation of the PI3K/Akt pathway and chemotherapeutic resistance. Drug Resist Updat 2002;5:234–48.
46. Fresno Vara JA, Casado E, de Castro J, et al. PI3K/Akt signalling pathway and cancer. Cancer Treat Rev 2004; 30:193–204.
47. Kumar R, Hung MC. Signaling intricacies take center stage in cancer cells. Cancer Res 2005;65:2511–5.
48. Read LC, Lemmey AB, Howarth GS, et al. The gastrointestinal tract is one of the most responsive target tissues for IGF-I and its potent analogs. In: Spencer EM, editor. Modern concepts of insulin-like growth factors. New York: Elsevier Science; 1991. p. 225–34.
49. Meroni PL, Raschi E, Testoni C, et al. Endothelial cell activation by antiphospholipid antibodies. Clin Immunol 2004;112:169–74.
50. Rotzschke O, Falk K, Strominger JL. Superactivation of an immune response triggered by oligomerized T cell epitopes. Proc Natl Acad Sci U S A 1997; 94:14642–7.

RAV12 Accelerates the Desensitization of Akt/PKB Pathway of Insulin-like Growth Factor I Receptor Signaling in COLO205

Jonathan Chi-Hang Li and Ronghao Li

Cancer Res 2007;67:8856-8864.